A simple integral approach to compute flows in ducts with variable cross-section

Bruno Audebert, Jean-Marc Hérard, Xavier Martin, Ouardia Touazi

A simple integral approach to compute flows in ducts with variable cross-section

Bruno Audebert, Jean-Marc Hérard, Xavier Martin, Ouardia Touazi

Keywords:
Finite Volumes/ well-balanced scheme / integral formulation / variable cross-section / Euler equations / Riemann problem.

Abstract We introduce in this paper a new approach based on an integral formulation in order to get a relevant approximation of the mean flow patterns in one-dimensional ducts with variable cross-sections. Numerical results are compared with those obtained by using the standard one-dimensional formulation associated with a well-balanced scheme, and also with numerical results provided by a multi-dimensional code. The comparison includes ducts with smooth or discontinuous cross sections. This new formulation is shown to be robust wrt to sudden and high

Bruno Audebert, Ouardia Touazi
EDF R&D, Fluid Dynamics, Power Energy and Environment, 6 quai Watier, F78400, Chatou.

Jean-Marc Hérard, Xavier Martin
EDF R&D, Fluid Dynamics, Power Energy and Environment, 6 quai Watier, F78400, Chatou,
and:

Institut de Mathématiques de Marseille, Equipe Analyse Appliquée, UMR CNRS 7353, 39 rue Joliot Curie, F13453 Marseille cedex 13.

Corresponding author : jean-marc.herard@edf.fr

cross-section variations, even when a total obstruction occurs, and to be accurate when compared with the reference solution.

1 Introduction

The approach that is classically retained in order to compute flows of a compressible fluid in variable cross-section ducts basically relies on the computation of approximate solutions of the following system of partial differential equations:

$$\begin{cases} \dfrac{\partial \rho S(x)}{\partial t} + \dfrac{\partial \rho u S(x)}{\partial x} = 0 \\ \dfrac{\partial \rho u S(x)}{\partial t} + \dfrac{\partial \rho u^2 S(x)}{\partial x} + S(x)\dfrac{\partial P}{\partial x} = D(W)S(x) \\ \dfrac{\partial E S(x)}{\partial t} + \dfrac{\partial u(E+P)S(x)}{\partial x} = 0 \end{cases} \tag{1}$$

where ρ, u, Q, P, E respectively denote the density, the velocity, the momentum ($Q = \rho u$), the pressure and the total energy of the fluid, when focusing on a single-phase model ; in this formulation, $S(x)$ stands for the cross-section area, and the total energy is:

$$E = \rho(\varepsilon(\rho, P) + U^2/2),$$

for a given equation of state where the internal energy $\varepsilon(\rho, P)$ is prescribed by the user. The contribution $D(W)$ enables to take regular head losses into account if necessary ; these may be due to viscous effects on the lower and upper wall boundaries of the duct. A classical closure law is in that case :

$$D(W) = -K(W)|u|u$$

where $K(W)$ is a positive scalar function. This one-dimensional approach is of course very useful in many practical and industrial situations, where there is no specific need to get a detailed evaluation of transverse components. This is true for many medical applications, for flows of oil-gas mixtures in pipelines in the oil industry, or water flows in complex networks for agriculture purposes or for electric companies. However, many practical situations often involve sudden contractions and/or enlargements of the duct cross-section. This in turn introduces two new difficulties. Firstly, one usually needs to introduce additional terms in the former system

in order to account for so-called singular head losses. Then one has to handle these generally stiff contributions when developing a numerical method.

Whenever additional source terms $D(W)$ are neglected or not, a generic numerical approach has been proposed some time ago, which is grounded on the well-balanced ideas introduced in [15]. Actually several useful and efficient algorithms have been proposed during the last twenty years in that direction. We may refer for instance to [15, 14, 13, 23, 20, 17, 19, 4, 16, 6], where the main ingredient consists in introducing a new fictitious variable $S(x,t)$, writing a new simple PDE:

$$\frac{\partial S}{\partial t} = 0.$$

At the discrete level, the cross section is assumed to be uniform within each Finite Volume cell. A straightforward consequence in that case is that the non-conservative term $S\frac{\partial P}{\partial x}$ in the momentum equation now clearly contributes to the convective budget. However, a first difficult point immediately arises, since one obviously needs to define appropriate and unique jump conditions around the sudden cross-section variations; a widespread approach consists in using a connection of states around the cross-section discontinuity, by enforcing the preservation of Riemann invariants of the standing wave. This makes sense for subsonic flows since the -single- field associated with the standing wave is linearly degenerated. A remaining difficulty for sonic and supersonic flows is about the non-uniqueness of solutions of the associated one-dimensional Riemann problem; for this specific problem of the -local in time- occurence of the resonance phenomenum, we refer for instance to [12]. As a matter of fact, it has been checked in [10] that the well-balanced Rusanov scheme introduced in [20] guarantees the convergence towards the unique subsonic solution, whereas standard schemes that do not satisfy the well-balanced property converge (when the mesh size tends to 0) towards a wrong solution. Another similar verification has been achieved in [16] when focusing on a well-balanced VFRoe-ncv scheme. On the whole, this means that suitable -well-balanced- numerical tools can

provide meaningful and convergent approximations of solutions of this system.

However, it has also been pointed out in [11] that the true multi-dimensional solutions do not comply with the modelling of the vicinity of the cross-section discontinuity. This indeed is not a very surprising result, and it was expected. Actually, noting as usual:

$$H = (E+P)/\rho,$$

a reasonable guess is that the mean axial momentum QS and the mean total energy flux QSH, which are two among the three Riemann invariants of the standing wave, are indeed preserved across any cross-section restriction; nonetheless, the failure in the modelling is due to the last Riemann invariant.

Thus, at least two possible ways to circumvent this problem may be suggested. A first one would consist in enforcing a local and singular momentum head loss, in order to recover the reality of the flow. This might be achieved by using relevant engineer closure laws (see for instance [18]), or by providing some adaptative and suitable closure law -to be defined-; in that case, one should also need to derive a new well-balanced scheme in order to preserve this new connection through the standing wave (see [8]). The second one, that is considered afterwards, is more straightforward: it simply consists in a reformulation of the one-dimensional problem, thus accounting for sudden variations in a very simple "multi-dimensional" spirit. A straightforward consequence is that singular sources are automatically computed. Another consequence is that this approach is valid for any EOS, and may be extended quite easily, for instance to the framework of multi-phase flow models.

Hence the paper is organised as follows. We first present the modified one-dimensional approach in section 2. Afterwards, we check that this formulation is suitable when one aims at computing approximate solutions of ρ, Q, E when the cross section is smooth. Next, we turn to unsteady approximate solutions obtained

in a sudden contraction/enlargement, and a comparison is made between:

1. the true multi-dimensional solution obtained on a very fine grid, which will be refered to as the ”reference” solution;
2. the classical one-dimensional well-balanced approach associated with the simulation of solutions of (1);
3. the new one-dimensional formulation, considering coarse or fine grids.

Several test cases are considered in that section. We will conclude by emphasizing the main advantages and drawbacks of the different one-dimensional approaches.

2 A simple one-dimensional Finite Volume scheme

In order to simplify the presentation, we focus in this paper on the inviscid Euler model for compressible flows of a single-phase fluid. Thus the main unknowns in a three-dimensional framework are the density ρ, the three components of the velocity $\underline{U}$ and of the momentum $\underline{Q} = \rho \underline{U}$, the pressure P and the mean total energy E:

$$E = \rho((\underline{u})^2/2 + \varepsilon(P,\rho)).$$

The speed of acoustic waves is:

$$\rho c^2 = \left(\frac{P}{\rho} - \rho \frac{\partial \varepsilon(P,\rho)}{\partial \rho} \right) / (\frac{\partial \varepsilon(P,\rho)}{\partial P})$$

with $\varepsilon(P,\rho)$ the internal energy given by the user. The governing equations read:

$$\begin{cases} \dfrac{\partial \rho}{\partial t} + \nabla.(\underline{Q}) = 0 \\ \dfrac{\partial \underline{Q}}{\partial t} + \nabla.(\underline{Q} \otimes \underline{u}) + \nabla P = 0 \\ \dfrac{\partial E}{\partial t} + \nabla.\left(\underline{Q} H\right) = 0 \end{cases} \tag{2}$$

where again the total enthalpy H is:

$$H = (E+P)/\rho$$

We consider control volumes as depicted on *Figure 1*, and we integrate (2) from time t^n to t^{n+1}. Thus, noting:

$$\Omega_i^{\varphi} = S_i \times h_i$$

the volume occupied by the fluid within the i-cell, we get at time $t = t_p$:

$$\Omega_i^{\varphi} \Phi_i^p = \int_{\Omega_i^{\varphi}} \Phi(\underline{x}, t_p) dv,$$

for: $\Phi = \rho, \underline{Q}, E$.

Using previous definitions, and noting Γ_i the boundary of the control volume Ω_i, standard calculations enable to derive the following update:

$$\left\{ \begin{array}{l} \Omega_i^{\varphi} \left(\rho_i^{n+1} - \rho_i^n \right) + \int_{[t^n, t^{n+1}]} \int_{\Gamma(i)} (\underline{Q}.\underline{n})(\underline{x}_{\Gamma}, t) d\Gamma dt = 0 \\ \Omega_i^{\varphi} \left(\underline{Q}_i^{n+1} - \underline{Q}_i^n \right) + \int_{[t^n, t^{n+1}]} \int_{\Gamma(i)} ((\underline{Q}.\underline{n})\underline{u} + P\underline{n})(\underline{x}_{\Gamma}, t) d\Gamma dt = 0 \\ \Omega_i^{\varphi} \left(E_i^{n+1} - E_i^n \right) + \int_{[t^n, t^{n+1}]} \int_{\Gamma(i)} ((\underline{Q}.\underline{n})H)(\underline{x}_{\Gamma}, t) d\Gamma dt = 0 \end{array} \right. \quad (3)$$

As shown in figure 1, the boundary $\Gamma(i) = \Sigma_j \Gamma_{ij}$ consists in three distinct parts corresponding to:

- (i) the upper and lower wall boundaries, through which the normal mass flux is null;
- (ii) $\Gamma_{i+1/2}^{\varphi}$ (respectively $\Gamma_{i-1/2}^{\varphi}$) where the fluid may flow in the x direction between cells i and $i+1$ (respectively between cells $i-1$ and i);
- (iii) walls boundaries aligned with the y direction between cell Ω_i and its neighbouring cells Ω_{i-1} and Ω_{i+1}, through which the normal mass flux is again equal to 0, and the surfaces of which are $max(0, (S_i - S_{i-1}))$ and $max(0, (S_i - S_{i+1}))$ respectively,

so that :

$$S_i = mes(\Gamma_{i-1/2}^{\varphi}) + max(0, (S_i - S_{i-1})) = mes(\Gamma_{i+1/2}^{\varphi}) + max(0, (S_i - S_{i+1})).$$

These definitions make sense, whatever the triple (S_{i-1}, S_i, S_{i+1}) is, even when one among these is equal to 0.

Thus, setting $\Delta t^n = t^{n+1} - t^n$, and denoting $V(i)$ the set of neighbouring cells of cell i, including the wall "mirror" cells associated with the wall boundaries of cell i, the Finite Volume scheme scheme is as follows:

$$\begin{cases} \Omega_i^{\varphi}\left(\rho_i^{n+1}-\rho_i^n\right)+\Delta t^n\sum_{j\in V(i)}(\underline{Q}.\underline{n})_{ij}^h\Gamma_{ij}=0 \\ \Omega_i^{\varphi}\left(\underline{Q}_i^{n+1}-\underline{Q}_i^n\right)+\Delta t^n\sum_{j\in V(i)}((\underline{Q}.\underline{n})\underline{u}+P\underline{n})_{ij}^h\Gamma_{ij}=0 \\ \Omega_i^{\varphi}\left(E_i^{n+1}-E_i^n\right)+\Delta t^n\sum_{j\in V(i)}((\underline{Q}.\underline{n})H)_{ij}^h\Gamma_{ij}=0 \end{cases} \tag{4}$$

In the latter formulation, the fluxes $(\phi)_{ij}^h$ denote suitable explicit numerical fluxes. These may be obtained using either a Godunov scheme, a Rusanov scheme or an approximate Godunov scheme. In practice, we will concentrate herein on a hybrid formulation where the numerical fluxes on fluid/fluid interfaces $\Gamma_{i+1/2}^{\varphi}$ will be obtained with the approximate Godunov scheme [9], and the numerical fluxes on fluid/solid interfaces will correspond to the exact Godunov fluxes. An alternative practical choice might be to replace the approximate Godunov scheme at fluid/fluid interfaces by a Rusanov (respectively exact Godunov) scheme, but this would of course decrease the overall accuracy (respectively increase the computational cost) of computations.

Before going further on, we introduce classical notations below:

$$\underline{\psi}.\underline{n_x}=\psi_x \qquad \underline{\psi}.\underline{n_y}=\psi_y$$

for $\underline{\psi}$ equal to $\underline{Q}$ or $\underline{u}$. We also assume that the initial condition at the beginning of the computation t^0 is such that the transverse velocity in the $y-$direction is null in all computational cells: ${U_y}_i^0=0$.

2.1 Mass and energy discrete balance equations

Since discrete normal fluxes are null at wall boundaries, the mass balance discrete equation is simply the following:

$$\Omega_i^{\varphi}\left(\rho_i^{n+1}-\rho_i^n\right)+\Delta t^n\left((\rho u_x)_{i+1/2}^h\Gamma_{i+1/2}^{\varphi}-(\rho u_x)_{i-1/2}^h\Gamma_{i-1/2}^{\varphi}\right)=0 \tag{5}$$

while noting:

$$\Gamma^{\varphi}_{i+1/2} = min(S_i, S_{i+1})$$

A similar straightforward calculation leads to the discrete energy balance equation:

$$\Omega^{\varphi}_i \left(E^{n+1}_i - E^n_i\right) + \Delta t^n \Big((\rho H u_x)^h_{i+1/2} \Gamma^{\varphi}_{i+1/2} - (\rho H u_x)^h_{i-1/2} \Gamma^{\varphi}_{i-1/2} \Big) = 0 \qquad (6)$$

2.2 Momentum balance discrete equations

We first prove that the flow remains such that the discrete y-momentum $(Q_y)^n_i$ remains null. Actually, the dot product of the second equation in 4 with the unit vector $\underline{j} = (0,1)$ yields:

$$\Omega^{\varphi}_i \left((Q_y)^{n+1}_i - (Q_y)^n_i\right) + \Delta t^n \sum_{j \in V(i)} ((\underline{Q}.\underline{n})(u_y) + P \underline{n}.\underline{j})^h_{ij} \Gamma^{\varphi}_{ij} = 0$$

For all wall boundaries, the Godunov scheme computes $(\underline{Q}.\underline{n})^h_{i,wall} = 0$; moreover, the exact Godunov scheme (or approximate Godunov scheme [9]) also provides zero contributions for fluxes $((\underline{Q}.\underline{n})(u_y))^h_{i\pm 1/2}$ on the vertical fluid/fluid interfaces $\Gamma^{\varphi}_{i\pm 1/2}$, as soon as u_y is equal to zero. On the other hand, the scalar product $\underline{n}.\underline{j}$ is null everywhere except on the lower and upper wall boundaries; however, the exact Godunov value of the wall pressure will be equal to the cell pressure as soon as $(u_y)^n_i$ is equal to zero; hence, the budget will cancel when summing up on both lower and upper frontiers. On the whole, we can conclude that:

$$\Omega^{\varphi}_i \left((Q_y)^{n+1}_i - (Q_y)^n_i\right) = 0$$

and thus :

$$(Q_y)^{n+1}_i = 0$$

if $(Q_y)^n_i = 0$. This completes the proof.

Eventually, the discrete $x-$momentum balance for $Q_x = \rho u_x$ will take the form:

$$\Omega_i^{\varphi}\left(Q_{x_i}^{n+1} - Q_{x_i}^{n}\right) + \Delta t^n\Big((\rho u_x^2 + P)_{i+1/2}^{h}\Gamma_{i+1/2}^{\varphi} - (\rho u_x^2 + P)_{i-1/2}^{h}\Gamma_{i-1/2}^{\varphi}\Big) + \Delta t^n P_{i+\frac{1}{2},i}^{*}\Big(S_i - \Gamma_{i+1/2}^{\varphi}\Big) - \Delta t^n P_{i-\frac{1}{2},i}^{*}\Big(S_i - \Gamma_{i-1/2}^{\varphi}\Big)\Big) = 0 \quad (7)$$

where $P_{i\pm\frac{1}{2},i}^{*}$ stands for an estimation of the pressure on the wall boundary $i \pm 1/2$.

On the whole, the set of equations (5),(7),(6) enables to update values of the density ρ, $x-$ moentum Q_x and total energy E.

2.3 Estimations of the pressure of the wall boundary

This estimation requires to specify the EOS. We give below formulas associated with a perfect gas EOS:

$$P = (\gamma - 1)\rho\varepsilon(P, \rho).$$

We get for $S_i > S_{i+1}$:

- if $M_i = \frac{u_i^n}{c_i^n} < 0$, then: $P_{i+\frac{1}{2},i}^{*} = \begin{cases} P_i^n\left(1 + \frac{\gamma-1}{2}M_i\right)^{\frac{2\gamma}{\gamma-1}} & \text{if } 1 + \frac{\gamma-1}{2}M_i \geq 0 \\ 0 & \text{otherwise} \end{cases}$
- if $M_i = \frac{u_i^n}{c_i^n} > 0$, then: $P_{i+\frac{1}{2},i}^{*} = P_i^n\left(1 + \gamma M_i\left(1 + \frac{(\gamma+1)^2}{16}M_i^2\right)^{1/2} + \frac{\gamma(\gamma+1)}{4}M_i^2\right)$

and a similar result holds when $S_i < S_{i+1}$.

Very similar results can be obtained when using a stiffened gas EOS -which is useful for almost incompressible flow calculations-, that is:

$$P + \gamma P_\infty = (\gamma - 1)\rho\varepsilon(P, \rho).$$

where P_∞ is a positive constant.

For more general EOS, more complex formulas may be obtained ([1]), using the Riemann invariant parametrization of the fast waves associated with $\lambda = u \pm c$ when $\underline{u}.\underline{n}_{wall} \leq 0$, and shock connections when the flow locally hits the wall boundary (when $\underline{u}.\underline{n}_{wall} > 0$).

2.4 Remarks

1. A first remark concerns other simpler estimations of the wall pressure. At first, it may be argued that $M_i = \frac{u_i^n}{c_i^n}$ in fact corresponds to the normal Mach number $\mathscr{M}_i = \frac{(\underline{u}.\underline{n})_i^n}{c_i^n}$; thus it is expected to be rather small, at least for fine enough meshes, since the mass flux $\underline{u}.\underline{n}$ is null at the wall boundary. Hence, it seems appealing to replace the exact Godunov value of the wall pressure by some rough approximation, setting M_i to 0, which yields:

$$P^*_{i+\frac{1}{2},i} = P_i^n$$

when $S_i > S_{i+1}$ whatever the sign of $(\underline{u}.\underline{n})_i^n$ is.

Even more, an obvious candidate for the wall pressure estimate can be provided by approximate Riemann solvers. For instance, the approximate Godunov scheme [9] computes a numerical wall pressure which is close to the one detailed above, since it computes:

$$P_{wall}^{VFRoe-ncv} = P_i^n \left(1 + \gamma M_i\right).$$

whenever M_i is positive or negative. As it can be easily noticed, this expression exactly corresponds to a first-order expansion of the exact Godunov value detailed above, with respect to the mach number M_i.

2. Another remark pertains to a suitable definition of the time step. Depending on the choice of numerical fluxes at the fluid interfaces, CFL-like conditions must be introduced in order to guarantee positive discrete values of the density ρ_i^n. For instance, when focusing of the Rusanov flux scheme:

$$f_{i+1/2}^n = \left(F(W_i^n) + F(W_{i+1}^n) - r_{i+1/2}^n (W_{i+1}^n - W_i^n) \right) /2$$

(where $r_{i+1/2}^n = max(r(W_i^n), r(W_{i+1}^n))$, and $r(W)$ stands for the spectral radius of the Jacobian matrix $\dfrac{\partial F(W)}{\partial W}$), the classical one-dimensional $CFL_{Rusanov}$ condition that guarantees $0 \leq \rho_i^{n+1}$ if $0 \leq \rho_i^n$ (for all cells):

$$\Delta t^n (r_{i+1/2}^n + r_{i-1/2}^n) \leq 2h_i$$

should be replaced by the following $CFL1D+_{Rusanov}$ condition on the time step:

$$\Delta t^n \left(r_{i+1/2}^n \Gamma_{i+1/2}^{\varphi} + r_{i-1/2}^n \Gamma_{i-1/2}^{\varphi} + u_i^n (\Gamma_{i+1/2}^{\varphi} - \Gamma_{i-1/2}^{\varphi}) \right) \leq 2\Omega_i^{\varphi}$$

This result can be classically obtained, using equation (5) and rewriting the latter in the form:

$$\rho_i^{n+1} = a_i^n \rho_i^n + b_i^n \rho_{i-1}^n + c_i^n \rho_{i+1}^n.$$

It can then be checked that both b_i^n and c_i^n are positive without any condition, whereas $0 \leq a_i^n$ if and only if the condition ($CFL1D+_{Rusanov}$) holds. Thus the new CFL condition is a little bit more restrictive than the one associated with the pure one-dimensional case; however, for smooth variations of the cross-section, we retrieve almost the same condition on the time step.

3 Numerical results

In the following next two subsections,we will discuss results that have been obtained while computing approximations of Euler equations for a compressible fluid.

The first subsection is devoted to the steady flow in a nozzle, restricting to the case where a shock occurs in the divergent part of the nozzle. This includes a study of the numerical convergence with respect to the mesh size.

The second subsection is the most important one, since it examines the behaviour of the present integral approach when computing the flow in a duct with a sudden contraction/enlargement. The latter subsection also contains a thorough comparison with:

- the reference solution obtained by computing the two-dimensional set of Euler equations on a very fine mesh, using the approximate Godunov scheme [9];

- the approximation obtained with the classical one-dimensional system (1), using the well-balanced scheme [20].

For all test cases, we have used a perfect gas equation of state, setting: $\gamma = 7/5$. In all cases the CFL constant has been set to $1/2$.

3.1 Steady flow in Laval nozzle

This flow is subsonic in the convergent part of the nozzle, sonic at the nozzle throat, supersonic before the shock location, and then subsonic until the exit. The approximate solution obtained with the integral approach is compared with the exact solution, which is classical and is not recalled herein. We emphasize that a very accurate treatment of inlet and outlet boundary conditions is mandatory in order to get a relevant approximation. For that topic we refer for instance to [1] and references

therein. Several meshes have been considered for that purpose ; we provide here numerical approximations corresponding to four meshes including 100, 1000, 10000 and 50000 cells respectively.

Inlet boundary conditions are derived using an upstream reservoir condition, where the fluid is at rest, and the pressure and total enthalpy are:

$$P_0 = 10^5 Pa \quad and \quad H_0 = 294615.75.$$

The outlet boundary condition is:

$$P_{outlet} = 75 \times 10^3 Pa.$$

Initial conditions are chosen as follows:

$$U_x(x,t=0) = 0, \quad P(x,t=0) = 10^5 Pa, \quad T(x,t=0) = 293.15K$$

The wall boundary estimate for the pressure in cell i is chosen as :

$$P^*_{i+\frac{1}{2},i} = P^*_{i-\frac{1}{2},i} = P^n_i.$$

Figures 2, 3, 4, 5 respectively provide the mean pressure, the density, the Mach number and the velocity of the fluid when the flow is steady, while restricting to Rusanov scheme. Computational results obtained with 100 and 50000 cells are provided, together with the exact steady solution. A comparison of convergence rates in L^1 norm for pressure, velocity and density variables obtained with Rusanov scheme and $VFRoe_{ncv}$ scheme is given on figure 6. The convergence rate is clearly 1 for both schemes, which was expected for this steady case with a first-order scheme. Obviously $VFRoe_{ncv}$ scheme is a bit more accurate than Rusanov scheme for a given mesh size. Of course, for this kind of application in smooth cross-section ducts,

many other schemes behave quite well too (see for instance [7, 23, 20, 4, 1], among others).

3.2 Unsteady flow of a compressible fluid with abrupt cross-section variations

We turn now to the computation of unsteady flows of a compressible fluid in duct including a sudden contraction/enlargement. A comparison of three distinct approaches is now considered.

- At first, a *reference solution* is computed, which corresponds to the simulation of the Euler equations 2 in a two-dimensional framework, using one million cells and the approximate Godunov scheme [9];

- We compute then approximations of the classical set of one-dimensional equations (1), using various meshes and the the well-balanced Rusanov scheme introduced in [20], the verification of which can be found in [10];

- The third series of approximations corresponds to the numerical approximations obtained with our integral approach, thus computing discrete values with (5),(7),(6) using coarse or fine one-dimensional meshes.

The experimental setup is a one-dimensional pipe with a sudden contraction located at $x_c = 0.8$ (see Figure 7). Thus the cross section is:

$$S(x < x_c) = S_l \quad and: \quad S(x > x_c) = S_r$$

When starting the computation, the initial membrane situated at $x_m = 0.7$ separates two distinct initial states (ρ_L, u_L, P_L) and (ρ_R, u_R, P_R). Depending on this choice, two situations may be considered.

In the first one, where:

$$(\rho_L, u_L, P_L) = (1, 0, 10^5)$$

and:

$$(\rho_R, u_R, P_R) = (0.125, 0, 10^4).$$

and restricting to the beginning of the computation, a right-going shock wave propagates towards the right direction, and is followed by a contact discontinuity; meanwhile, a rarefaction wave travels towards the left boundary. Then the right-going *shock* wave hits the sudden contraction, and a reflected wave and a transmitted wave respectively travel to the left and right side of the contraction $x = x_c$.

Of course, left and right initial states (ρ_L, u_L, P_L) and (ρ_R, u_R, P_R) can be permuted. In that case, the *smooth* right-going rarefation wave interacts with the sudden contraction; again two reflected and transmitted waves occur.

We examine these two configurations in the sequel; moreover, two different cross-section ratios are considered in this subsection:

$$S_l/S_r = 2$$

and:

$$S_l/S_r = 100$$

The finest (respectively coarsest) one-dimensional mesh that is used for both the classical approach -with the well-balanced scheme- and the integral approach contains 50000 (respectively 100) regular cells.

The pressure estimate that is used for all computations at the wall-boundary is either the rough approximation retained in the former subsection:

$$P^*_{i+\frac{1}{2},i} = P^*_{i-\frac{1}{2},i} = P^n_i.$$

or the more accurate Riemann wall-boundary expression detailed in section 2.3.

3.2.1 A shock wave hits a section contraction

First test case 1: $S_l/S_r = 2$:
This corresponds to a rather classical situation arising in many practical simulations. We plot on Figure 8 the density profiles at time $t = T_0 = 1.5 \times 10^{-3}$. We note that:

- The red and green curves correspond to the integral approach when using a mesh with 50000 (respectively 1000) cells ; the blue curve refers to the approximation obtained with the wall estimate of the pressure provided in section 2.3 with the finer mesh;

- Approximations associated with the magenta curve have been obtained with the classical approach and the well-balanced scheme;

- The black curve gives the mean value of the reference solution in the section.

When using the rough approximation of the wall pressure, (thus setting M_i to 0 in formulas of section 2.3), it appears that the integral approach provides a very nice approximation of the reference solution, which is indeed much better than the classical approach with the well-balanced scheme. This remains true even when the mesh is coarse (see figure 8, with one thousand cells). We also plot the velocity/pressure/entropy profiles on figures 9, 10, 11. Similar comments hold when comparing the three approaches (reference solution, integral approach and classical approach). Figure 12 gives the behaviour of the wall pressure estimate (rough estimate $P_{wall} = P^n_i$ and Riemann value detailed in section 2.3) wrt time, and it also provides a comparison with the wall pressure computed by the code that solves two-

dimensional Euler equations.

Second test case: $S_l/S_r = 100$:

When the cross-section contraction is much higher, the well-balanced scheme fails at providing approximations as soon as the shock wave hits this contraction. We emphasize that the same trouble arises when using the well-balanced approximate Godunov scheme [16]. In practice, when the numerical shock wave hits the contraction, the non linear solver that computes values of the density solution of $f_{-,+}(\rho) = 0$ on both sides of cell interfaces (see [20] and also, [16] section 3.2, [10] appendix C, or [11] appendix D) no longer finds any positive solution. Tentative cures that enforce the minimal value ρ_{min} such that $f_{-,+}(\rho_{min}) = min_{x \in R^+} f_{-,+}(x)$ also lead to a failure of the code.

For this second test case, we thus only compare profiles:

- when using the integral approach and a mesh including 50000 cells: the black **dotted** curve displays results corresponding to the rough wall pressure estimate $P_{wall} = P_i^n$ in cell i at time t^n, and the black **dashed** curve refers to the approximation obtained with the wall pressure estimate in section 2.3;

- The black curve gives the mean value of the reference solution in the section.

Actually, computational approximations are close to one another in this second test case (see figure 13). The comparison with the reference multi-dimensional solution is really fair. This is also true for the remaining pressure/velocity components. Figure 14 is the counterpart of the previous one Figure 12 for this second test case; the three estimates of the wall pressure hardly differ in that case, which was expected due to the high cross section contraction.

3.2.2 A rarefaction wave hits a section contraction

The experimental setup is still the same, but initial states on both sides of the membrane are now:

$$(\rho_L, u_L, P_L) = (0.125, 0, 10^4)$$

and:

$$(\rho_R, u_R, P_R) = (1, 0, 10^5).$$

The cross section is the same as in test case 1, which means that:

$$S_l/S_r = 2$$

This test is interesting, since the incoming wave that meets the sudden contraction is smooth now (it is a right-going rarefaction wave). Thus one expects that more or less, all computations will lead to similar results. We emphasize that the well-balanced scheme computes this situation, on any mesh, and hence we can again compare on figure 15:

- Results obtained with the integral approach when using a mesh with 50000 cells, and considering the exact Riemann estimate for the wall pressure or its rough approximation $P_{wall} = P_i^n$ in cell i at time t^n ;

- Approximations associated with the classical approach and the well-balanced scheme;

- The y averaging of the reference two-dimensional solution.

We can observe velocity and pressure numerical approximations on Figures 16 and 17. We also recall the basic Riemann solution (in yellow) at some earlier time $t = 0.131 \times 10^{-3}$ when the position x_r of the head of the right-going rarefaction wave is smaller than x_c. Figure 18 also details the wall pressure computed by the two slightly different integral approaches. Once more, the prediction provided by

the classical approach and the well-balanced scheme is far less accurate than the integral approach, whatever the wall pressure estimate is. This remains unchanged independently of the mesh refinement. In particular, the reflected wave (for $x < x_c$) has not the correct tendencies, whereas the transmitted wave (for $x > x_c$) is rather good in all situations.

4 Conclusion

Focus has been given in this paper on the one-dimensional approximation of single-phase fluid flows, but obviously, this approach may be extended to two-phase flow models in a straightforward manner. This is for instance true for standard conservative homogeneous models, but also for Baer-Nunziato type models ([3, 5]). Nonetheless, in the latter case, the occurence of non-conservative terms in the multi-dimensional model introduces an additional small difficulty that can be managed rather easily in a meaningful way. The present one-dimensional Finite Volume approach is very simple and rather efficient, as it has been shown in section 3. This claim is also confirmed by numerous computations described in [22], where sixteen different situations have been investigated, considering eight contractions:

$$S_l/S_r = \frac{1}{100}; \quad \frac{1}{10}; \quad \frac{1}{2}; \quad \frac{9}{10};$$

and:

$$S_l/S_r = \frac{10}{9}; \quad 2; \quad 10; \quad 100.$$

Scheme $FV1D+$ simply relies on an integral formulation on specific Finite Volumes, and it requires to give a suitable approximate value of the wall pressure in the multi-dimensional framework. It has been emphasized herein that the local -in cell- value of the pressure is indeed a fair candidate.

Moreover, it has been pointed out that, in some situations involving high ratios of the cross-section between two neighbouring cells, the well-balanced schemes may fail at providing approximations, whatever the mesh size is. This is an important remark, since one expects to get approximations that will converge uniformly towards the true solution when some sudden closure of the duct occurs. Actually, the present one-dimensional Finite Volume approach enables to achieve this requirement in a continuous way, without introducing any difficulty.

Another consequence of the present work is that some new approach may be considered in order to define a meaningful and direct approach for the tricky problem of the homogeneisation of obstacles in industrial components arising in nuclear power plants ([21]). This work is currently under way ([2]). Eventually, we would like to emphasize that, as mentionned in the introduction, some counterpart of the classical well-balanced formulation, which takes advantage of the present results, is also currently investigated. We expect that this work will help improving the classical well-balanced strategy.

Acknowledgements Xavier Martin benefits from financial support through an EDF-CIFRE contract 2012/0838. This work has been achieved within the framework of the TITANS2 project. All computational facilities were provided by EDF. Authors also thank Erwan Lecoupanec and Thomas Pasutto for their help with Code_Saturne.

References

1. Audebert, B. and Blondel, F. and Pasutto, T. and Stanciu, M., Condensation models and boundary conditions for non-equilibrium wet steam flows, *International Journal on Finite Volumes, http://www.latp.univ-mrs.fr/IJFV/*, pp.1-52, vol.10, 2013.
2. Audebert, B. and Hérard, J.-M. and Martin, X. and Ouardia, T., Une formulation pour la prise en compte des obstacles en milieu encombré, *internal EDF report*, 2014.
3. Baer, M. R. and Nunziato, J. W., A two-phase mixture theory for the deflagration-to-detonation transition (DDT) in reactive granular materials., *International journal of multiphase flow*, pp.861-889, vol.12,1986.
4. Clain, S. and Rochette, D., First and second-order Finite Volume methods for the one-dimensional non-conservative Euler system, *Journal of Computational Physics*, pp.8214-8248, vol.228, 2009.
5. Coquel, F. and Gallouët, T. and Hérard, J. M. and Seguin, N., Closure laws for a two-fluid two-pressure model , *Comptes Rendus Mathematique*, pp.927-932, vol.334,2002.
6. Coquel, F. and Saleh, K. and Seguin, N., A robust and entropy-satisfying numerical scheme for fluid flows in discontinuous nozzles, *Mathematical Models and Methods in Applied Sciences*, pp.2043-2083, vol.24,2014.
7. Faucher, E. and Hérard, J.-M. and Barret, M. and Toulemonde, C. , Computation of flashing flows in variable cross-section ducts, *International Journal of Computational Fluid Dynamics*, pp. 365-391, vol.13, 2000.
8. Galié, T., Couplage interfacial de modèles en dynamique des fluides. Application aux écoulements diphasiques , *PhD thesis, Universit Pierre et Marie Curie-Paris VI*, 2009.
9. Gallouët, T. and Hérard, J.-M. and Seguin, N., On the use of symetrizing variables for vacuums., *Calcolo*, pp.163-194, vol.40, 2003.
10. Girault, L. and Hérard, J.-M., A two-fluid hyperbolic model in a porous medium., *ESAIM : Mathematical Modelling and Numerical Analysis*, pp.1319-1348, vol.44, 2010.
11. Girault, L. and Hérard, J.-M. , Multidimensional computations of a two-fluid hyperbolic model in a porous medium., *International Journal on Finite Volumes, http://www.latp.univ-mrs.fr/IJFV/*, pp.1-33, vol.7, 2010.
12. Goatin, P. and LeFloch, P. G., The Riemann problem for a class of resonant hyperbolic systems of balance laws, *Annales de l'Institut Henri Poincare (C) Non Linear Analysis*, pp.881-902, vol.21, 2004.
13. Gosse, L., A well-balanced scheme using non-conservative products designed for hyperbolic systems of conservation laws with source terms, *Mathematical Models and Methods in Applied Sciences*, pp.339-365, vol.11, 2001.

14. Gosse, L. and Leroux, A. Y., Un schéma-équilibre adapté aux lois de conservation scalaires non-homogènes, *Comptes rendus de l'Académie des sciences. Srie 1, Mathématique*, pp.543-546, vol.323, 1996.
15. Greenberg, J.-M. and Leroux, A.-Y., A well-balanced scheme for the numerical processing of source terms in hyperbolic equations., *SIAM Journal on Numerical Analysis*, 1996, pp.1-16, vol.33.
16. Helluy, P. and Hérard, J.-M. and Mathis, H., A well-balanced approximate Riemann solver for compressible flows in variable cross-section ducts., *Journal of Computational and Applied Mathematics*, pp.1976-1992, vol.236, 2012.
17. Hérard, J.-M. , A rough scheme to couple free and porous media, *International Journal on Finite Volumes, http://www.latp.univ-mrs.fr/IJFV/*, pp.1-28, 3, 2006.
18. Idel'Cik, I. E., Memento des pertes de charge, *Collection de la Direction des Etudes et Recherches d'Electricite de France, Paris: Eyrolles*, 1969.
19. Kröner, D. and LeFloch, P. and Thanh, M. D. , The minimum entropy principle for compressible fluid flows in a nozzle with discontinuous cross-section., *ESAIM : Mathematical Modelling and Numerical Analysis*, pp.425-443, vol.42, 2008.
20. Kröner, D. and Thanh, M. D. , Numerical solutions to compressible flows in a nozzle with variable cross-section., *SIAM Journal on Numerical Analysis*, 2006, pp.796-824, vol.43.
21. Le Coq, G. and Aubry, S. and Cahouet, J. and Lequesne, P. and Nicolas, G. and Pastorini, S. , The THYC computer code. A finite volume approach for 3 dimensional two-phase flows in tube bundles, *Bulletin de la Direction des études et recherches-Electricité de France. Série A, nucléaire, hydraulique, thermique. In french*, pp.61–76, 1989.
22. Martin, X. , Numerical modeling of flows in obstructed media , *PhD thesis, Université Aix Marseille*, in preparation.
23. Rochette, D. and Clain, S. and Buffard, T. , Numerical scheme to complete a compressible gas flow in variable porosity media, *International Journal of Computational Fluid Dynamics*, pp. 299-309, vol.19,2005.

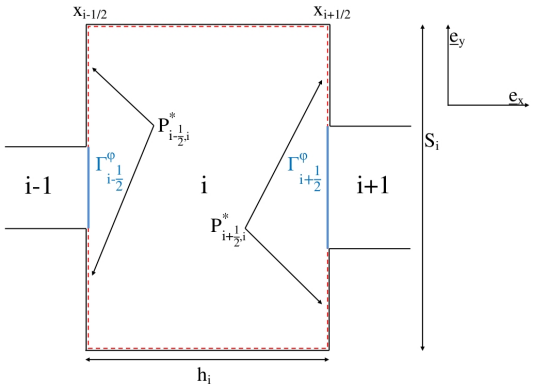

Fig. 1 Finite volume Ω_i with neighbouring cells, fluid interfaces and inner wall-boundaries.

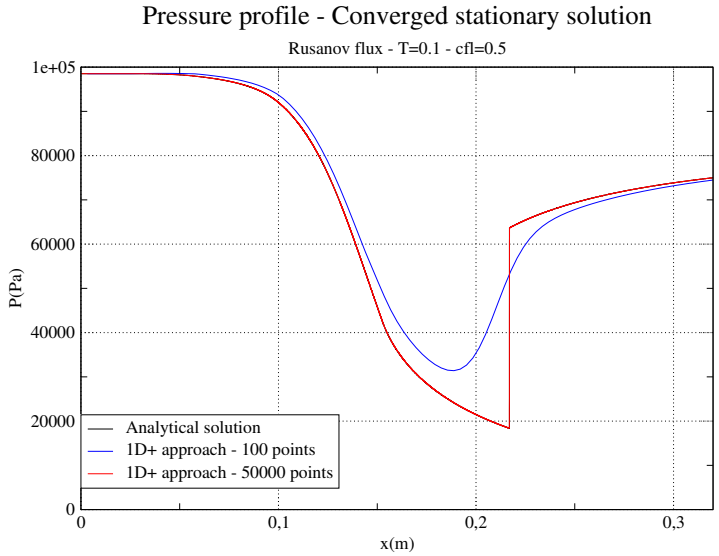

Fig. 2 Steady flow in Laval nozzle: pressure profile obtained with Rusanov scheme and 100 or 50000 cells.

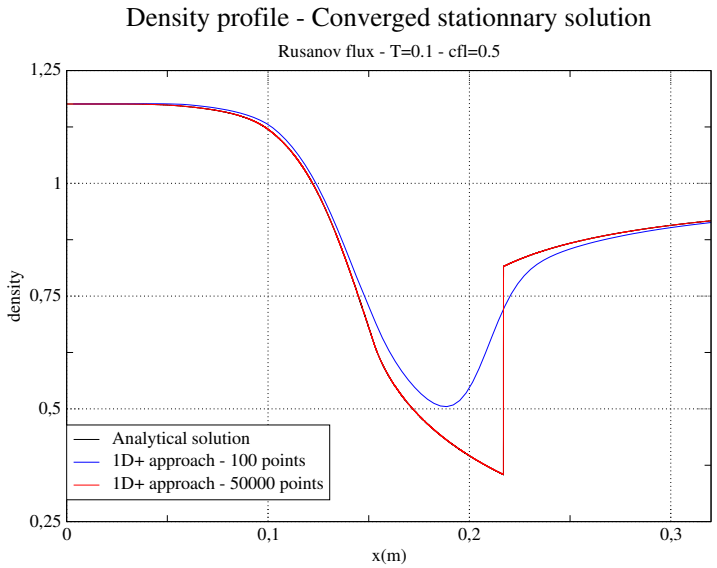

Fig. 3 Steady flow in Laval nozzle: density profile obtained with Rusanov scheme and 100 or 50000 cells.

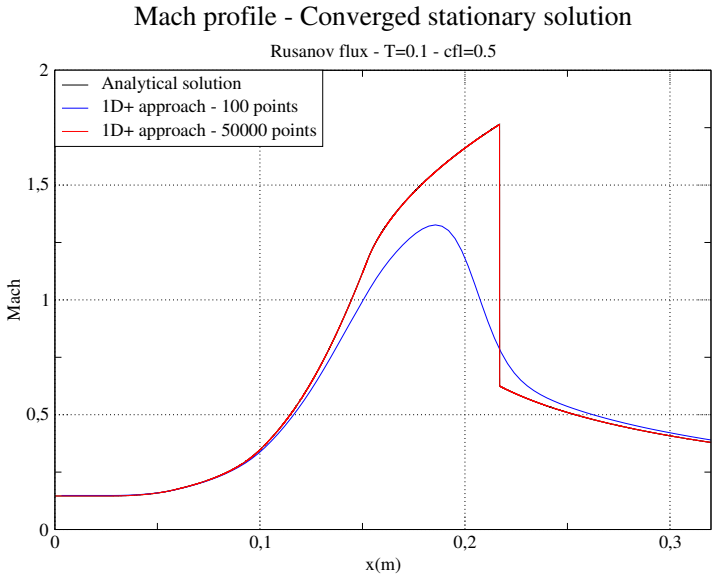

Fig. 4 Steady flow in Laval nozzle: Mach number profile obtained with Rusanov scheme and 100 or 50000 cells.

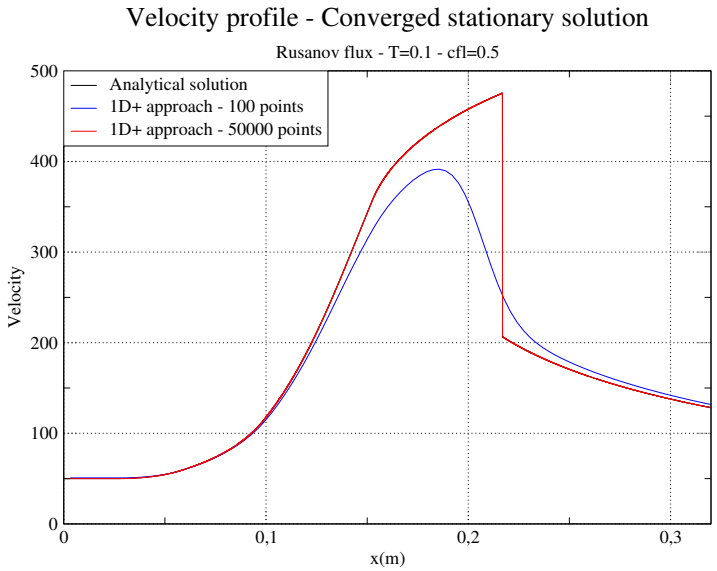

Fig. 5 Steady flow in Laval nozzle: velocity profile obtained with Rusanov scheme and 100 or 50000 cells.

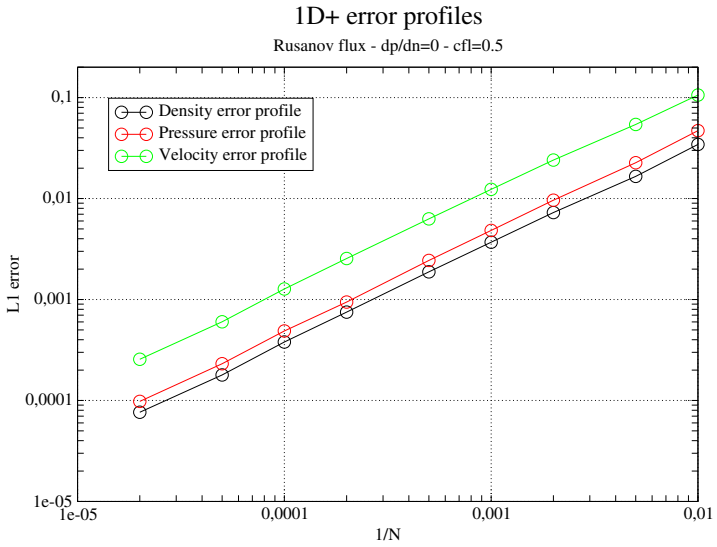

Fig. 6 Steady flow in Laval nozzle: L^1 norm of the error when using Rusanov and $VFRoe_{ncv}$ schemes. Coarser and finer meshes include 100 or 50000 cells.

Fig. 7 Experimental setup : 1D pipe with a sudden contraction and position of the initial membrane.

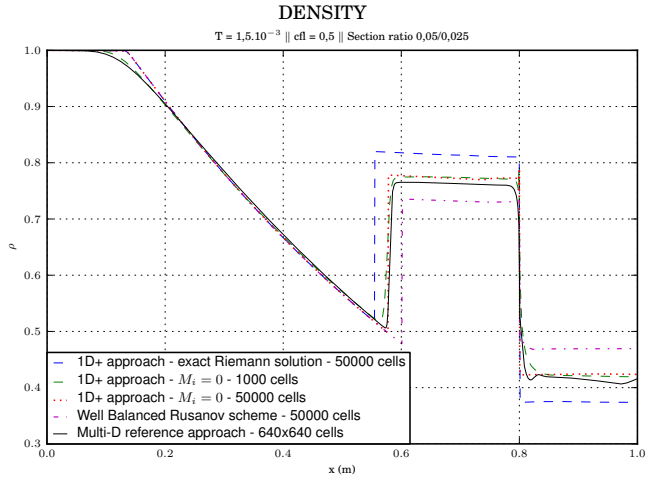

Fig. 8 Density profiles at $t = T_0$ in test case 1. Dashed blue curve: integral approach with 50000 cells, using the exact Riemann estimate of the wall pressure. Dotted red and dashed green curves: integral approach with 50000 and 1000 cells respectively, assuming $M_i = 0$ in wall pressures. Dotted-dashed magenta curve: well-valanced Rusanov scheme with 50000 cells. Black curve: $y-$averaging of 2D results.

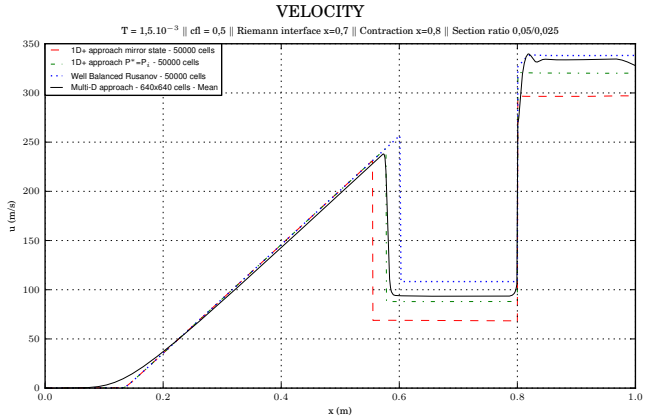

Fig. 9 Velocity profiles at $t = T_0$ in test case 1. Dashed red curve: integral approach with 50000 cells, using the exact Riemann estimate of the wall pressure. Dotted-dashed green curves: integral approach with 50000 cells , assuming $M_i = 0$ in the wall pressure estimate. Dotted blue curve: well-valanced Rusanov scheme with 50000 cells. Black curve: $y-$averaging of 2D results.

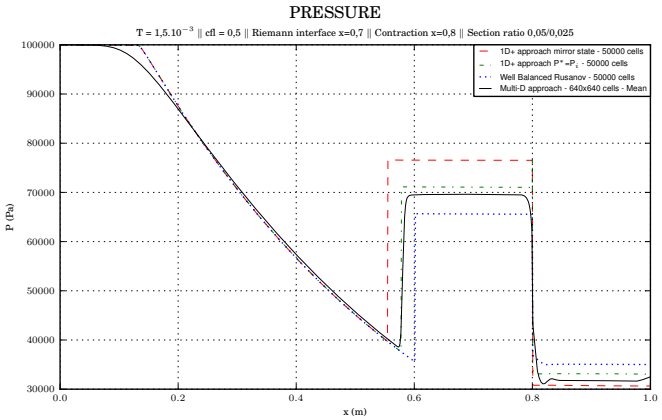

Fig. 10 Pressure profiles at $t = T_0$ in test case 1. Dashed red curve: integral approach with 50000 cells, using the exact Riemann estimate of the wall pressure. Dotted-dashed green curves: integral approach with 50000 cells , assuming $M_i = 0$ in the wall pressure estimate. Dotted blue curve: well-valanced Rusanov scheme with 50000 cells. Black curve: $y-$averaging of 2D results.

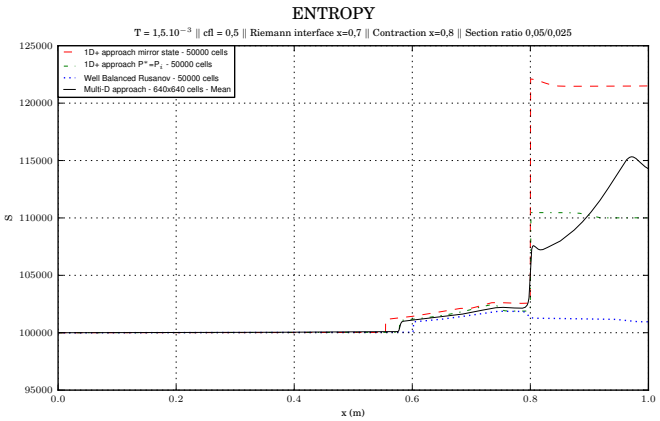

Fig. 11 Entropy profiles at $t = T_0$ in test case 1. Dashed red curve: integral approach with 50000 cells, using the exact Riemann estimate of the wall pressure. Dotted-dashed green curves: integral approach with 50000 cells , assuming $M_i = 0$ in the wall pressure estimate. Dotted blue curve: well-valanced Rusanov scheme with 50000 cells. Black curve: $y-$averaging of 2D results.

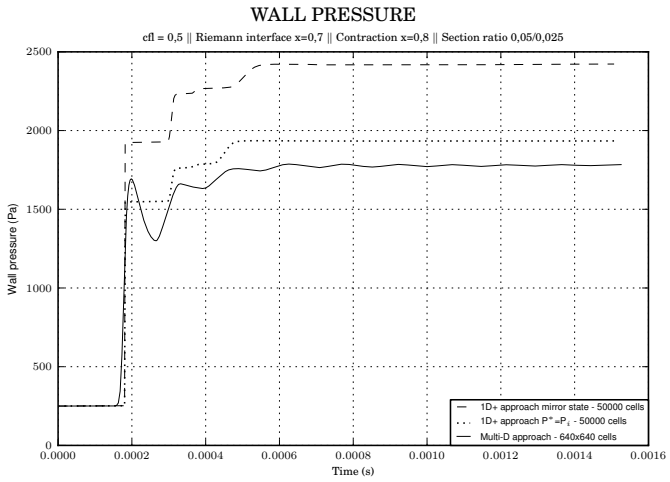

Fig. 12 Comparison of wall pressures in test case 1. Dashed curve: integral approach using the exact Riemann estimate of the wall pressure. Dotted curve: integral approach setting $M_i = 0$. Full black curve: multidimensional computation using 640^2 cells.

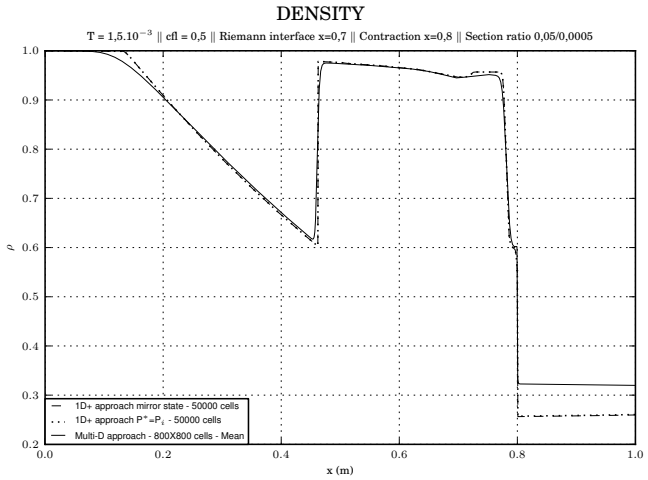

Fig. 13 Density profiles at $t = T_0$ in test case 2. Dashed curve: integral approach using the exact Riemann estimate of the wall pressure. Dotted curve: integral approach assuming $M_i = 0$ in wall pressure estimations. Black curve: $y-$averaging of two-dimensional results.

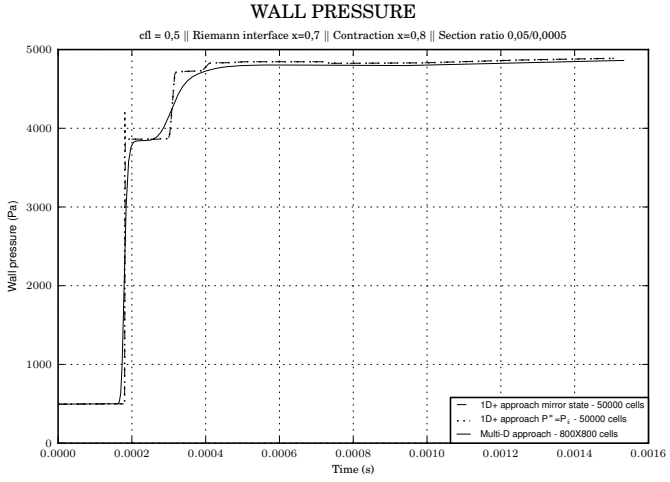

Fig. 14 Comparison of wall pressures in test case 2. Dashed curve: integral approach using the exact Riemann estimate of the wall pressure. Dotted curve: integral approach setting $M_i = 0$. Full black curve: multidimensional computation using 800^2 cells.

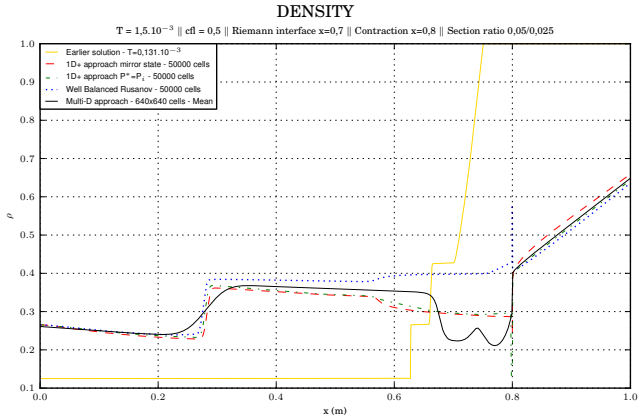

Fig. 15 Density profiles at $t = T_0$ in test case 3. Dashed curve: integral approach using the exact Riemann estimate of the wall pressure. Dotted curve: integral approach assuming $M_i = 0$ in wall pressure estimations. Black curve: $y-$averaging of two-dimensional results.

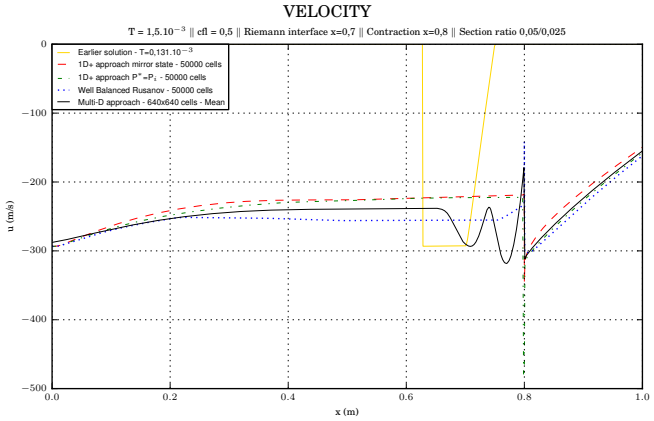

Fig. 16 Velocity profiles at $t = T_0$ in test case 3. Dashed curve: integral approach using the exact Riemann estimate of the wall pressure. Dotted curve: integral approach assuming $M_i = 0$ in wall pressure estimations. Black curve: $y-$averaging of two-dimensional results.

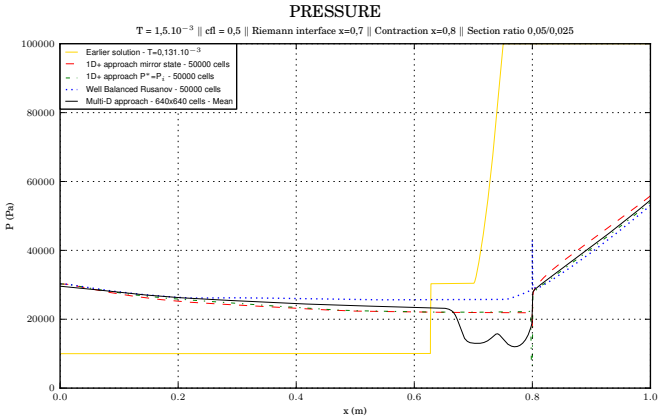

Fig. 17 Pressure profiles at $t = T_0$ in test case 3. Dashed curve: integral approach using the exact Riemann estimate of the wall pressure. Dotted curve: integral approach assuming $M_i = 0$ in wall pressure estimations. Black curve: $y-$averaging of two-dimensional results.

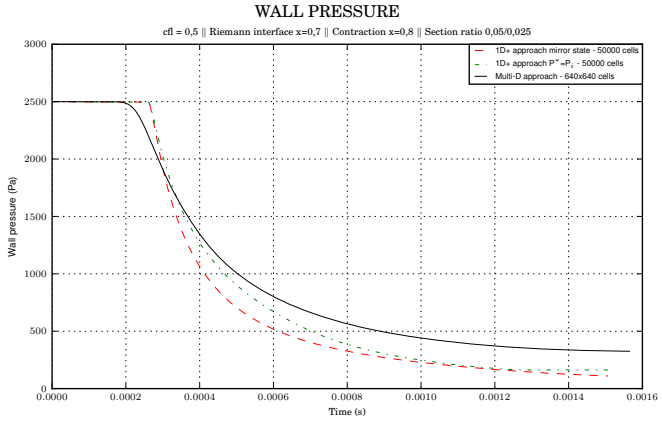

Fig. 18 Comparison of wall pressures in test case 3. Dashed curve: integral approach using the exact Riemann estimate of the wall pressure. Dotted curve: integral approach setting $M_i = 0$. Full black curve: multidimensional computation using 800^2 cells.